Journal of Alloys and Compounds 695 (2017) 726–736

Contents lists available at ScienceDirect

Journal of Alloys and Compounds

journal homepage: http://www.elsevier.com/locate/jalcom

Facile route to produce spherical and highly luminescent Tb^{3+} doped Y_2O_3 nanophosphors

Deepak Kumar [a], Manoj Sharma [b, c], D. Haranath [d], O.P. Pandey [a, *]

[a] School of Physics and Materials Science, Thapar University, Patiala, 147003, Punjab, India
[b] Department of Nanotechnology, Sri Guru Granth Sahib World University, Fatehgarh Sahib, 140406, Punjab, India
[c] UNAM–Institute of Materials Science and Nanotechnology, Bilkent University, Ankara, 06800, Turkey
[d] CSIR- National Physical Laboratory, Dr. K. S. Krishnan Road, New Delhi, 110012, India

ARTICLE INFO

Article history:
Received 15 December 2015
Received in revised form
26 May 2016
Accepted 14 June 2016
Available online 16 June 2016

Keywords:
Optical materials
Co-precipitation
Phosphor
Luminescence

ABSTRACT

Terbium doped yttrium oxide (Y_2O_3:Tb^{3+}) nanophosphor has been synthesized via a facial yet modified co-precipitation method. To get maximum luminescence output from Y_2O_3:Tb^{3+} nanophosphors, surfactants namely, Cetyl trimethylammonium bromide (CTAB) and Trioctylphosphine oxide (TOPO) were added during synthesis. Further, it has been observed that combined addition of surfactant (CTAB + TOPO) at the time of synthesis has resulted in nearly spherical morphology of the nanophosphor. Furthermore, these optimized material are observed to have enhanced integrated photoluminescence (PL) intensity of ~23% as compared to the one synthesized without the addition of any surfactant. The results are further supported by detailed structural and optical studies. Optimum use of surfactants during synthesis shows for the first time that both nano-sized distribution and high crystallinity can be achieved simultaneously which has resulted in bright green emission in Tb^{3+} doped Y_2O_3 nanophosphors.

1. Introduction

Nanocrystalline particles exhibit many novel physical properties not found in bulk materials [1,2]. These nanoparticles are of significant interest from the fundamental point of view for the phosphor's technological applications. Rare-earth compounds, such as hydroxides, oxides, phosphates, fluorides, and vanadates have been extensively studied because of their potential applications in the high-performance magnets, luminescent devices, catalysts, and other functional materials based on their electronic, optical, and chemical characteristics arising from the 4f electrons [3,4]. Among various rare-earth oxides, yttrium oxide (Y_2O_3) is a promising alternative host matrix for luminescence, which has a great application prospect in commercial lighting and display devices, due to its high chemical stability, low thermal expansion and phonon energy [5,6]. Luminescent properties of an optical host strongly depend on the structure and morphology of the crystals. By adjusting different morphologies of the host material, the relative intensity of the emission peaks can be effectively controlled. Therefore, the controllable synthesis of Y_2O_3 with well-defined morphology and narrow size distribution via a rapid, simple, and mass production method is a great challenge. To date, numerous efforts have been made to explore various convenient and efficient approaches for the preparation of different inorganic crystals in nano-dimensions with different shapes [7–9]. In these techniques, the use of organic additives as the shape modifier is a common strategy to adjust and control the morphology and size of the products. Organic molecules are known to either promote or inhibit crystal growth by modifying its surface. By properly choosing organic additives that might have specific molecular complementarity with their inorganic counterparts, the growth of the crystals can be rationally directed to yield products with desirable morphologies and/or hierarchical structures [10].

In many recent papers, an increase in PL efficiency with decrease in particle size in Tb^{3+} doped Y_2O_3 nanophosphors has been reported [11,12]. In fact unique physical behavior can be predicted in these systems as the particle size is reduced to become comparable to some characteristic lengths such as the Bohr's exciton radius [13]. Besides these commonly known quantum size effects, the excited states of the localized dopant atoms e.g., Tb^{3+} in Y_2O_3 can be strongly modulated because of quantum confinement in the

* Corresponding author.
E-mail address: oppandeytu@gmail.com (O.P. Pandey).

http://dx.doi.org/10.1016/j.jallcom.2016.06.124
0925-8388/

nanoparticles. These modifications result in changes in the overlap of wave functions with other atoms in the quantum dots [12]. Owing to this intonation consequence of quantum confinement, the impurity states in a doped nanocrystal (DNC) can interact more efficiently with the host than in the bulk, leading to momentous deviations in the electronic energy structure and transition probabilities [14]. Therefore, for improving the interaction of the dopant impurities with the host matrix, quantum confined nanostructures are desired, which is the main focus of in this work.

In the current work, we report the synthesis of Y_2O_3:Tb^{3+} as an efficient green-emitting nanophosphor by modified co-precipitation method. CTAB/TOPO with different combinations have been used as surfactants (during synthesis) in order improve the morphology and luminescence of the nanophosphor. The structural, morphological and luminescent properties were studied using X-ray diffractometer (XRD), Fourier transform infrared spectroscopy (FT-IR), High resolution transmission electron microscope (HRTEM), steady state and time resolved photoluminescence (PL) measurement techniques. XRD studies and Rietveld refinement confirmed the body-centered cubic structure of doped phosphors. With systematic structural and optical characterizations it has been observed that addition of CTAB or TOPO has enhanced the luminescent intensity of Y_2O_3:Tb^{3+} nanophosphors. Further, their combined addition (CTAB + TOPO) at the same time has helped to synthesize nano-sized highly luminescent Y_2O_3:Tb^{3+} green phosphor under UV excitation. Both luminescence and crystallinity were significantly improved, with the addition of these two surfactants simultaneously at the time of synthesis. These modifications in the synthesis route have resulted to achieve enhanced luminescence from Y_2O_3:Tb^{3+} nanophosphors along with high crystallinity and almost spherical morphology which increases the potentiality of this green phosphor in biological fields and innovative display applications.

2. Experimental

2.1. Materials

For synthesis, $Y(NO_3)_3.6H_2O$ (99.99%), $Eu(NO_3)_3.6H_2O$ (99.99%), Cetyl trimethylammonium bromide (CTAB) (99.99%), Trioctylphosphine oxide (TOPO) (99.99%) were purchased from Sigma Aldrich. Ammonium hydrogen carbonate (NH_4HCO_3) was purchased from Himedia. All the materials were used in as received condition without further purification.

2.2. Method

First, according to the formula $(Y_{0.995}Tb_{0.005})_2O_3$, stoichiometric amounts of rare-earth nitrates were dissolved in double distilled water and solution of 0.2 mol/L concentration was used as mother solution. Similarly, solutions of CTAB (0.001, 0.002, 0.003 and 0.004 mol%) and TOPO (0.005, 0.010, 0.015 and 0.025 mol%) as surfactant were prepared by adding proper amount of these surfactants in 30 mL of water. The surfactant solution was then added to mother solution and stirred for 30 min to form a homogeneous solution. 1.5 mol/L solution of ammonium hydrogen carbonate was used as precipitant. Under continuous stirring the precipitating solution was added into the mother solution till the pH of the solution reaches 7, resulting in formation of precipitates. The suspensions after 12 h of aging were centrifuged, washed 2 times with ethanol and 3 times with hot deionized water. Then it was filtered and dried at 75 °C for 24 h to get the white amorphous powders. These powders were sintered at 700 °C for 2 h in a tubular furnace at a heating rate of 1 °C per min in a recrystallized alumina boat to get the corresponding nano crystalline powders.

Out of the above prepared samples, Y_2O_3:Tb^{3+} (0.05 mol%) have shown maximum luminescence at 0.003 mol% and 0.015 mol% concentration of CTAB and TOPO, respectively (discussed later in context). Interestingly we have prepared one more sample of Y_2O_3:Tb^{3+} (0.05 mol%) with both CTAB (0.003 mol%) and TOPO (0.015 mol%) together as surfactant using similar synthesis route as discussed above.

For better understanding we have given codes to all sample prepared above in Table 1.

2.3. Characterization

X-ray diffraction (XRD) studies were carried out using Philips powder X-ray diffractometer (model PW 1071) with Ni filtered Cu K_α radiation in a wide range of Braggs angle 2θ ($15 \leq 2\theta \leq 85$). TEM images were recorded using JEOL 2100F (200 kV). For TEM analysis synthesized powder was dispersed in ethanol and ultra-sonicated for 15 min. One drop of the dispersed particles was put on a carbon-coated Cu grid and ethanol was allowed to evaporate. It was then mounted inside the sample chamber. Optical absorption spectra of the synthesized nanophosphors were recorded with double beam UV–Visible spectrophotometer using Hitachi U3900H in the range 200–700 nm. Photoluminescence study, calculation of Commission Internationale de l'Éclairage (CIE) color coordinates and Correlated Color Temperature (CCT) of the synthesized samples (in powder form) has been recorded with Edinburgh Instruments FLS920 spectrometer equipped with 450 W Xenon Arc Lamp and a cooled single photon counting photomultiplier (Hamamatsu R2658P). The lifetime measurement was carried out using a time-resolved luminescence spectrometer (model: F900 Edinburgh), equipped with a time correlated single photon counting system and microsecond xenon flash lamp as the source of excitation. FTIR spectra have been recorded in the range of 4000–400 cm^{-1} with Perkin Elmer Spectrum BX(2). The pH value of the precipitating solution was monitored using a calibrated Elico LI 120 pH meter. All the measurements were performed at room temperature (~20 °C).

3. Results and discussions

3.1. XRD phase analysis

3.1.1. Structural analysis

The phase and purity of the samples were studied by X-ray

Table 1
Detail of sample(s) along with their code(s).

S. No.	Name of the sample	Code
1	Y_2O_3:Tb^{3+} $_{(0.05\ mol\%)}$ at 700 °C	S_P
2	Y_2O_3:$Tb^{3+}_{(0.05\ mol\%)}$ + $CTAB_{(0.003\ mol\%)}$ at 700 °C	S_C
3	Y_2O_3:$Tb^{3+}_{(0.05\ mol\%)}$ + $TOPO_{(0.015\ mol\%)}$ at 700 °C	S_T
4	Y_2O_3:$Tb^{3+}_{(0.05\ mol\%)}$ + $CTAB_{(0.003\ mol\%)}$ + $TOPO_{(0.015\ mol\%)}$ at 700 °C	S_{CT}

P – pure (no additive), C- CTAB, T- TOPO, CT- CTAB + TOPO.
All the above samples are prepared at 700 °C.

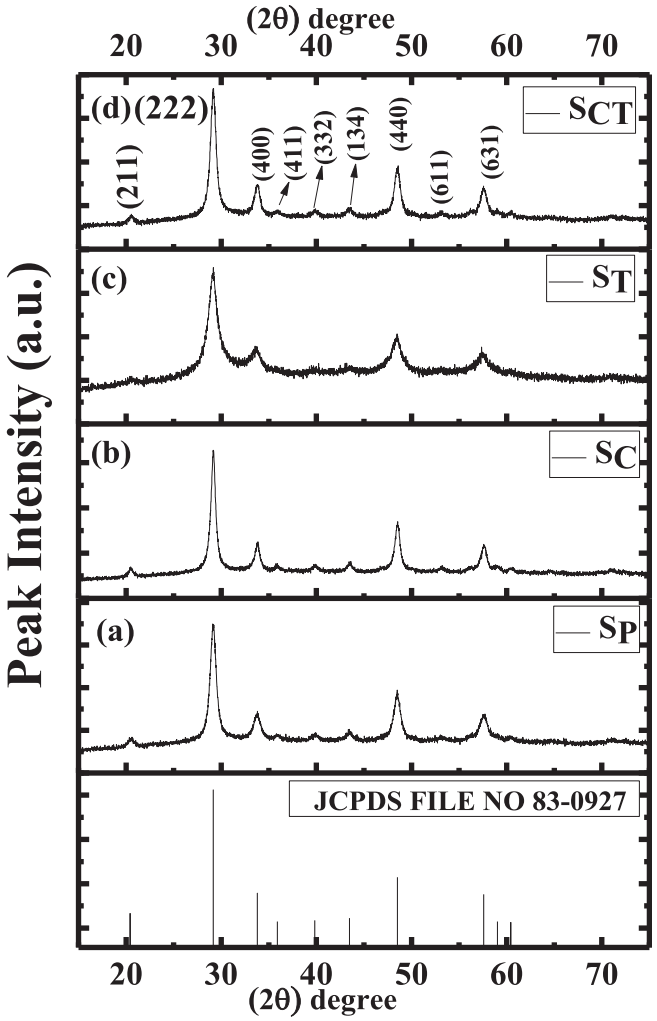

Fig. 1. (a–d): XRD pattern of (a) S_P, (b) S_C, (c) S_T and (d) S_{CT} samples.

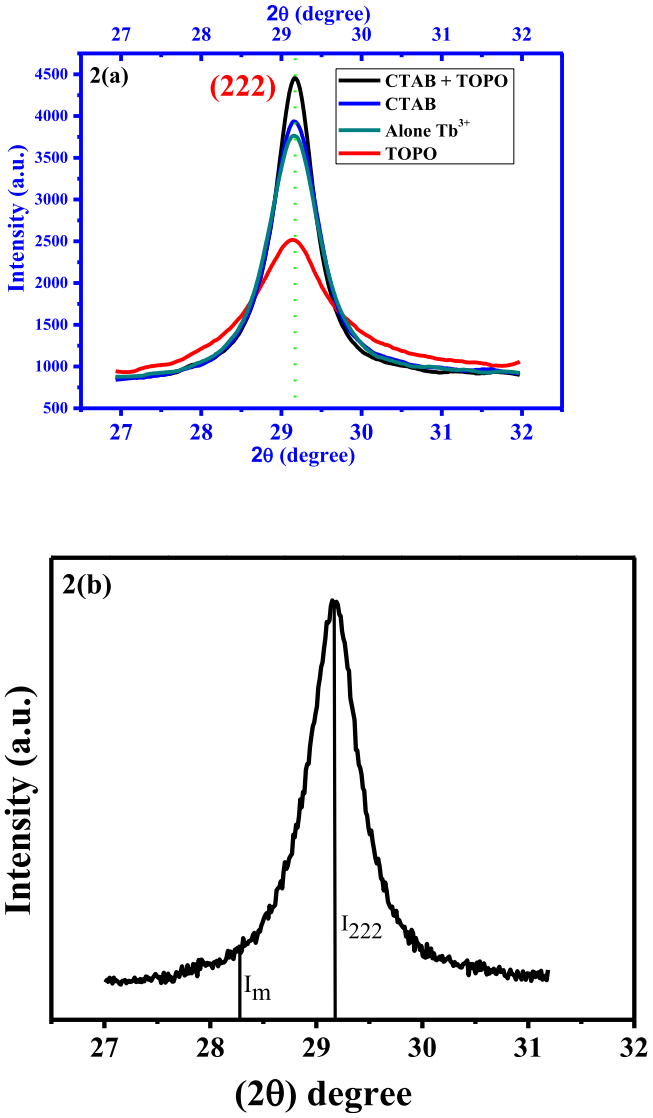

Fig. 2. (a) Comparative intensity of (2 2 2) diffraction peaks in the range of $2\theta = 27°–32°$ of these samples (a) S_P, (b) S_C, (c) S_T and (d) S_{CT}. (b) Crystallinity index (CI %) calculation from (222) peak.

power diffraction (XRD) measurement. Fig. 1(a–d) shows the XRD profiles of (a) S_P, (b) S_C, (c) S_T and (d) S_{CT} at 700 °C. For comparison purpose we have also given the XRD profile of pure cubic phase Y_2O_3 (JCPDS 83-0927) [15]. From these profiles one can see that samples prepared were in good agreement with the standard data of the pure cubic phase Y_2O_3 with space group Ia3 [15]. No impurity peak was observed in these XRD patterns, indicating high purity of the synthesized samples. No peak was observed for the dopant (Tb^{3+}) signifying complete substitution of Tb^{3+} ion in Y_2O_3 matrix. It further implies that the dopant ions have occupied the cationic sites in the host lattice [16]. The (hkl) values of the most prominent peaks are shown in the XRD pattern (Fig. 1(a–d)). To study the effect of surfactant on the crystallite size and crystallinity of the Y_2O_3:Tb^{3+}, we have selected the highest intensity peak (2 2 2) of all the samples (S_P, S_C, S_T and S_{CT}) from Fig. 1(a–d) and compared them in Fig. 2(a). A careful comparison of the (2 2 2) diffraction peak for samples (S_P, S_C, S_T and S_{CT}) between $2\theta = 27°–32°$ have shown the following observation (Table 2, Fig. 2(a)).

- The presence of TOPO at the time of synthesis in the samples (S_T) have caused broadening in (222) peak with decrease in peak intensity as compared to sample S_P.
- The sample containing CTAB as surfactant i.e. (S_C) have shown enhancement in peak intensity of this (222) peak with smaller broadening as compared to sample S_P.

It is important to mention here that, both these samples (S_T and S_C) were heated at same temperature (700 °C), for same time (2 h) under same physical condition and XRD measurements were also done under similar conditions. So based on the above observations it shows that CTAB surfactant during annealing helps in vanishing unwanted phases in the samples which are present before annealing. However, TOPO has decreased the crystallite size of the samples which results in the broadening of (222) peak. We have also observed the same behavior in all other peaks present in XRD of these samples (S_C and S_T) (Table 2). Interestingly in sample (S_{CT}) synthesized by adding CTAB and TOPO together, both the broadening and peak intensity of diffraction peaks were high i.e. this sample (S_{CT}) has smaller crystallite size and better crystallinity than the other prepared samples (S_T, S_C and S_P). From Table 2 we can see that for the sample S_T FWHM is more and peak intensity is less, and

Table 2
FWHM and Peak intensity of these samples (a) S_P, (b) S_C, (c) S_T and (d) S_{CT}.

Sample codes	(h k l)								
	(222)			(400)			(440)		
	FWHM (radian)	Peak intensity (a.u.)	2θ (degree)	FWHM (radian)	Peak intensity (a.u.)	2θ (degree)	FWHM (radian)	Peak intensity (a.u.)	2θ (degree)
S_C	0.67305	4568	29.16	0.67855	1711	33.78	0.68787	2363.3	48.52
S_T	1.17373	2606	29.16	1.55304	1288	33.49	1.33057	1400	48.40
S_{CT}	0.76162	4100	29.16	0.71828	1600	33.77	0.7819	2271	48.50
S_P	0.43922	3620	29.15	0.36903	1544	33.76	0.42426	2000	48.49

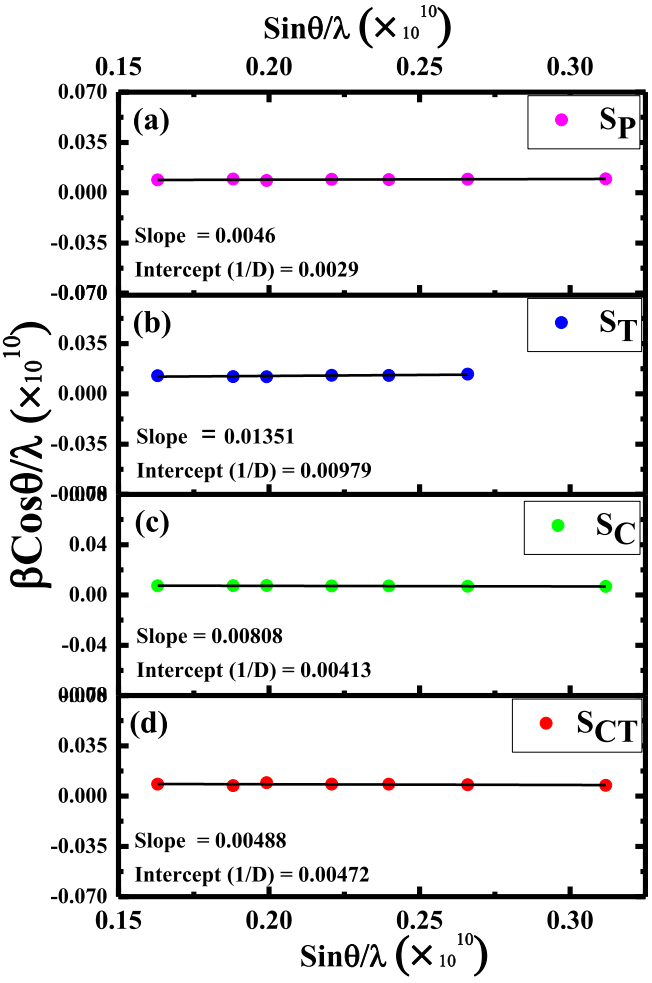

Fig. 3. (a–d): Hall–Williamson's plots.

for the sample S_C FWHM as well as peak height is high, as compared to S_P (which was prepared by adding no surfactant at the time of synthesis) sample.

To compare the crystallinity of the prepared samples, XRD crystallinity index (CI_{XRD}) were calculated from the following peak height method developed by Segal et al. [17].

$$CI_{XRD}(\%) = \frac{I_{222} - I_m}{I_{222}} \times 100 \quad (1)$$

where, I_{222} was the intensity of the (222) crystalline peak at 29° and I_m the height of the minimum of peak (222), as shown in Fig. 2(b) [17].

To investigate further, crystallite size (D in nm) was calculated using the Debye– Scherer formula [18] (Equation (2)) and the Hall–Williamsons method (Equation (3)) [19].

$$D = \frac{0.9\lambda}{\beta cos\theta} \quad (2)$$

$$\frac{\beta Cos\theta}{\lambda} = \frac{1}{D} + \frac{\varepsilon Sin\theta}{\lambda} \quad (3)$$

Here, β represents the full-width at half-maximum (FWHM) in radians, θ is the angle of the corresponding diffraction peak and λ (0.154 nm) is the wavelength of X-rays, ε represents the microstrain present in the samples. The crystallite size from the Hall–Williamsons equation (Equation (3)) was calculated from the reciprocal of the intercept of its straight line plot, as shown in Fig. 3 (a–d) for samples (a) S_P, (b) S_T, (c) S_C and (d) S_{CT}. The slope of this equation implies the micro-strain (ε) present in the samples. Table 3 illustrates the values of D (crystallite size in nm) and CI_{XRD} (%) of synthesized samples using above mentioned methods. Gaussian fitting was used to calculate the FWHM and height of peak (peak intensity) corresponding to hkl values of all the samples by origin pro software [20].

3.1.2. Rietveld refinement

To know the cubic nature of structure, a structural refinement by the Rietveld method [21] was performed using the Fullprof Program [22]. The structural refinement results for the samples (a) S_P, (b) S_C, (c) S_T and (d) S_{CT} phosphor annealed at 700 °C are shown in Fig. 4 (a–d) and are presented in Table SI (Supporting data). Results show good agreement between the observed and calculated XRD patterns. Quality of structural refinement data was checked by measuring a parameter called goodness of fit (GOF), which is defined as GOF = R_{wp}/R_{exp} [22,23]. For perfect refinement the GOF must approach unity. In the present case, the GOF for samples (a) S_P,

Table 3
Illustrates the values of D (crystallite size in nm) and CI_{XRD} (%).

Sample code	CI_{XRD} (%) (crystallinity index)	D (crystallite size) nm	
		Debye Scherer ± error	Hall–Williamson's ± error
S_{CT}	80.1	18 ± 0.30	20 ± 0.24
S_T	64.3	17 ± 0.15	15 ± 0.21
S_C	77.2	25 ± 0.22	24 ± 0.37
S_P	70.2	36 ± 0.38	34 ± 0.51

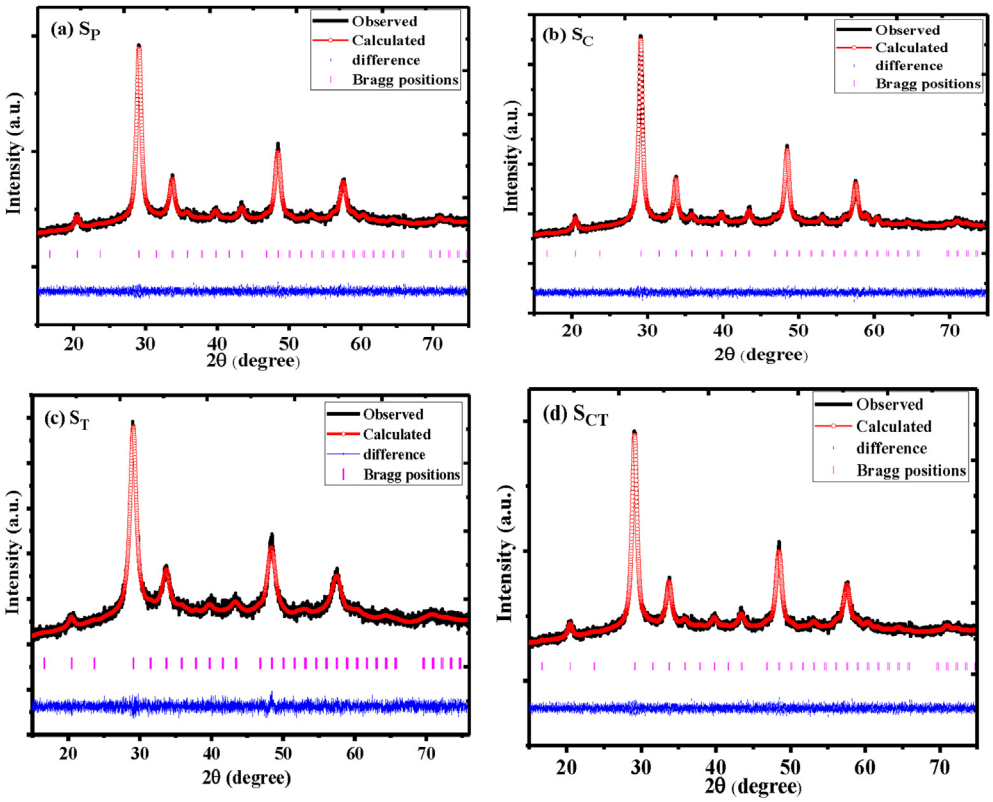

Fig. 4. (a–c): Refinement data of (a) S_C, (c) S_T and (d) S_{CT} sample.

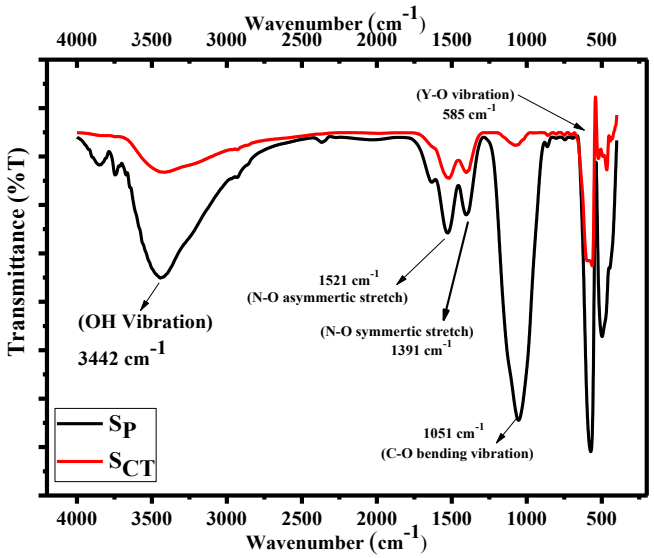

Fig. 5. FTIR of samples S_P and S_{CT}.

(b) S_C, (c) S_T and (d) S_{CT} was found to be 1.20, 1.24, 1.21 and 1.33. Detailed discussions related to crystallographic data and modeling of unit cell using Rietveld refinement data are presented in supporting data section (section A, Figure SI(a, b) and Table S1).

3.2. FTIR analysis

FTIR study has been performed for the samples S_P and S_{CT} as shown in Fig. 5. A broad IR band at 3442 cm^{-1} corresponds to OH stretching vibration [24]. This band for the S_{CT} sample becomes comparatively small. The absorption band due to O–H vibration is absent in the commercial undoped Y_2O_3 phosphor [16]. The residual hydroxyl groups (–OH) at 3442 cm^{-1} quenches the emission intensity in rare earth emission and decreases the luminescence intensity. This band becomes weaker with increase in annealing temperature and disappears at higher temperatures. During synthesis since both these samples were sintered at same temperature (700 °C) so this difference between the peaks may be due to better crystallinity of the S_{CT} sample as compared to S_P (discussed in XRD earlier). This band becomes weaker with increase in annealing temperature [24] (disappears at higher temperatures) and by modifications during synthesis (washing the sample several time by ethanol and water before annealing) [25]. The nitro group around 1519 cm^{-1} and 1404 cm^{-1} has also displayed a decrease in S_{CP} sample as compared to S_P. The residual nitro group around 1500 cm^{-1} are called luminescence quenchers for rare earth emission and decreases the luminescence emission intensity [26–29]. These facts discussed above support that the use of polymers i.e. CTAB and TOPO at the time of synthesis and during sintering which has decreased the luminescent quenchers to a greater extent which has resulted highly luminescent Y_2O_3:Tb^{3+} phosphors.

3.3. TEM micrographs

Fig. 6 (a–d) shows the TEM micrographs of (a) S_P, (b) S_T, (c) S_C and (d) S_{CT} nanophosphors sintered at 700 °C. In Fig. 6(a) agglomerated particles can be seen as no additive was used at the time of synthesis. For sample S_T flake like morphology can be observed in Fig. 6(b). Few folded flakes can be seen as samples were heated at 700 °C temperature. Spherical morphology of the

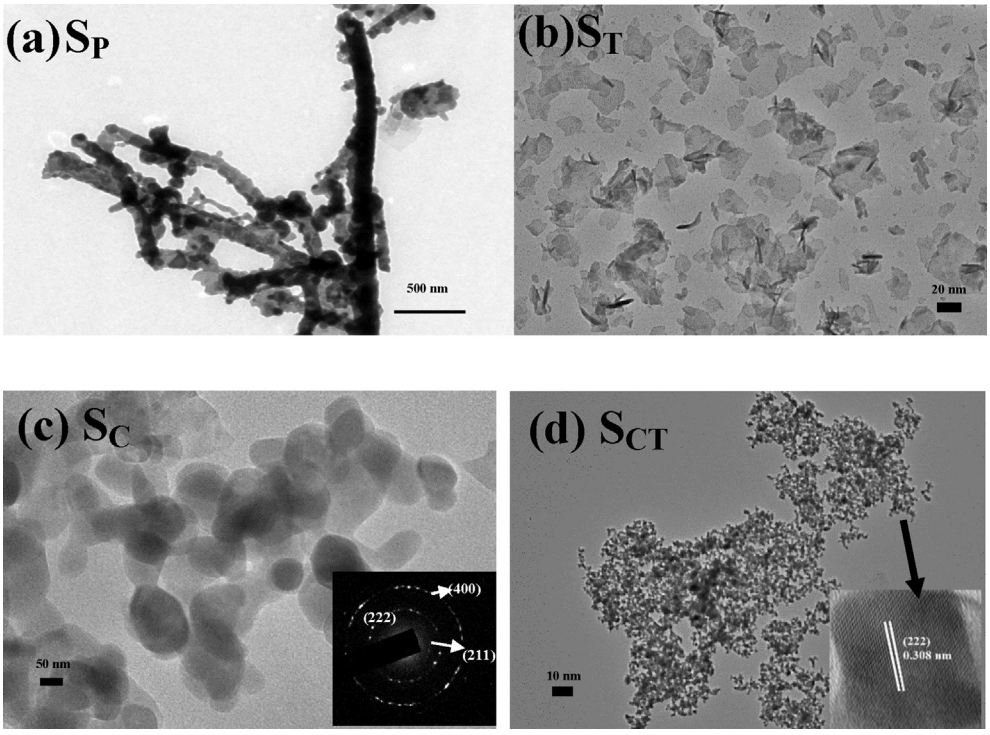

Fig. 6. (a–d): TEM image of (a) S_P, (b) S_T, (c) S_C and (d) S_{CT} sample.

particles can be seen in samples S_C as shown in Fig. 6(c). Average particle diameter calculated from Fig. 6(c) lies between 30 and 40 nm which matches well with XRD measurements discussed earlier. Fig. 6(d) represents TEM micrographs corresponding to sample S_{CT}. Since both the surfactants (CTAB + TOPO) were present at the time of synthesis, this sample (S_{CT}) has shown almost spherical morphology having particle diameter lying between 15 and 25 nm which agrees well with XRD data. The inset of Fig. 6(c) shows Selected Area Electron Diffraction (SAED) pattern of S_C sample. Observed ring instead of spots corresponds to nanocrystalline nature of synthesized phosphor. The observed rings corresponding to (211), (222) and (400) lattice planes of the cubic phase of Y_2O_3 are shown in inset of Fig. 6(c), which are in good agreement with the XRD patterns discussed before. Inset of Fig. 6(d) for sample S_{CT} shows lattice fringes (0.308 nm) corresponding to (222) which further defends its crystalline behavior.

3.4. Photoluminescence studies

To understand the effect of surfactant on optical properties of Tb^{3+} doped Y_2O_3, we have recorded Photo luminescence excitation and emission spectra of various synthesized samples. Fig. 7(a, b) represents the comparative emission spectra of samples S_P vs S_T and S_P vs S_C under excitation of 267 nm. Inset of Fig. 7(a, b) shows the intensity relation with concentration of corresponding surfactant. Enhancement in PL emission intensity due to addition of surfactant at the time of their synthesis as compared to sample S_P can be observed. The obtained optimal concentration for maximum luminescence in sample S_C and S_T is 0.003 mol% (CTAB) and 0.010 mol% (TOPO) respectively. Peak position in the emission spectra (Fig. 7(a, b)) does not change with surfactant concentration suggesting that the nature of Tb^{3+} activator remains unchanged with concentration of surfactant. Percentage increase in PL emission intensity of S_T and S_C samples w.r.t. pure sample S_P is 2.34% and 1.49% respectively. It has also been seen (inset of Fig. 7 (a, b)) that as the concentration of surfactant increases above its optimum concentration, PL intensity decrease thereafter [30]. Fig. 8(a, b) represents excitation and emission spectra of S_P, S_C, S_T and S_{CT} samples. Excitation spectrum recorded at $\lambda_{em} = 545$ nm emission is the overlapping bands having maxima at 267 and 301 nm [31,32]. The band at around 267 nm is ascribed to the O^{2-}/Tb^{3+} charge transfer band (CTB), which corresponds to the electronic transitions from the 2p orbital of O^{2-} to the 4f orbital of Tb^{3+}. Origin of the band at 301 nm results from absorption of incident radiation by Tb^{3+} ions and leads to excitation of electrons from Tb^{3+} ground state to one of its excited 4f levels [16]. However, due to the parity forbidden character of the transition within the 4f configuration, the peaks beyond 301 nm were weak [32,33]. Emission spectra of Y_2O_3: Tb^{3+} (1.0 mol%) (Fig. 7(a, b), 8(b)) is composed of several sharp lines resulting due to the $^5D_4 \rightarrow {}^7F_J$ transitions where J = 3, 4, 5 and 6. Strongest emission occurs at 545 nm due to the $^5D_4 \rightarrow {}^7F_5$ characteristic transition of green emission for Tb^{3+} [16,32]. The other peaks at 485 nm, 585 nm and 625 nm arise from the $^5D_4 \rightarrow {}^7F_6$, $^5D4 \rightarrow {}^7F_4$ and $^5D_4 \rightarrow {}^7F_3$ transitions, respectively. Band-gap diagram of Y_2O_3:Tb^{3+} is given in Fig. 9. The emission intensity of S_{CT} sample has shown large enhancement. Percentage improvement in PL intensity in this sample S_{CT} is 23% as compared to sample S_P which was prepared without addition of any surfactant (Fig. 8(b)).

3.4.1. Decay analysis

Further, to understand behavior of luminescent decay, the decay data was fitted with different decay equations (Fig. 10(a–d)). It was found that curve follow second order exponential decay for the prepared samples [34–36].

$$I(t) = I_0 + I_1 e^{-1/\tau 1} + I_2 e^{-1/\tau 2} \quad (4)$$

Where I_1 and I_2 are intensities at different times and their corresponding lifetimes are τ_1 and τ_2 respectively. The average lifetime can be calculated using the relation [36].

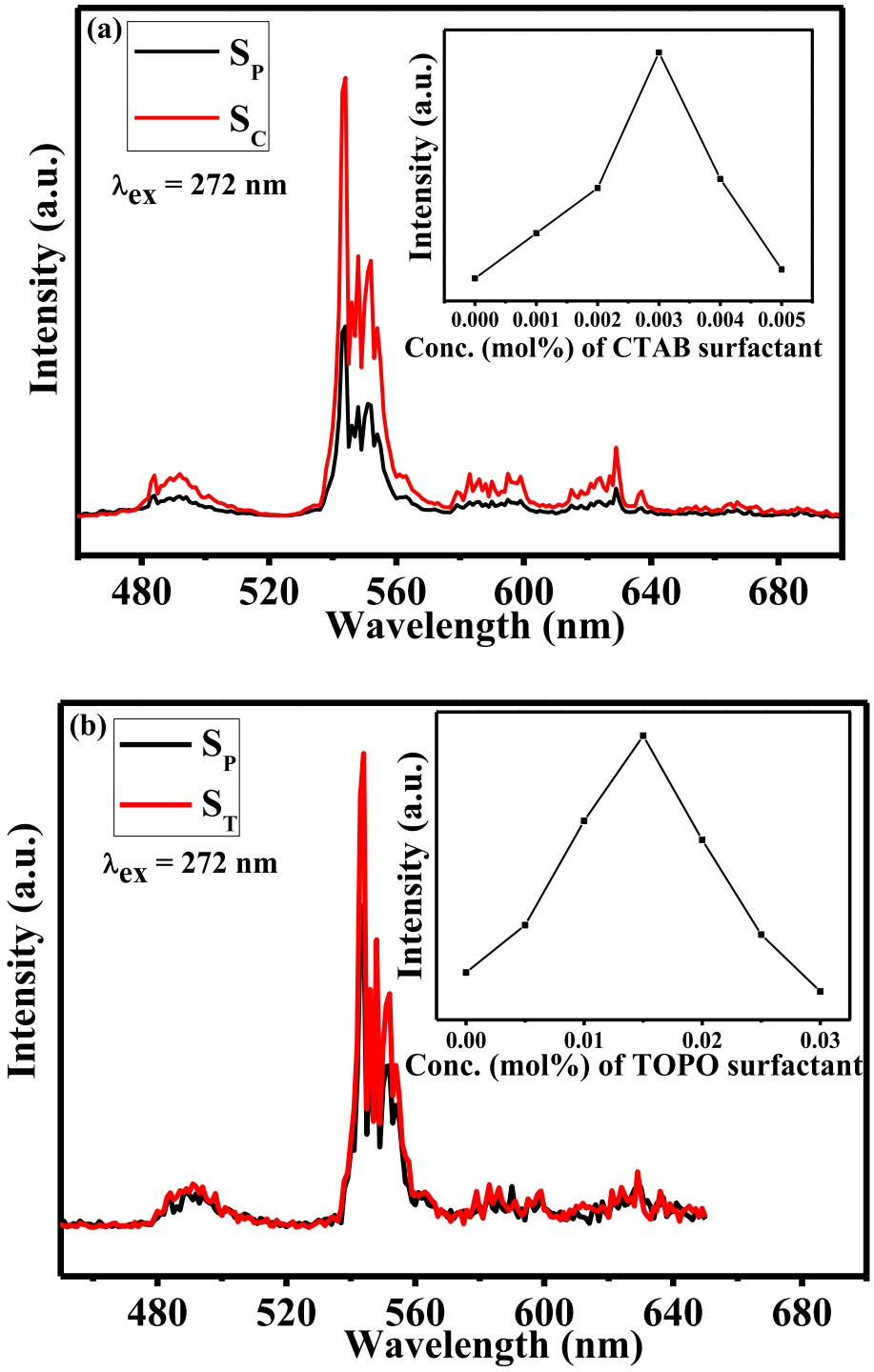

Fig. 7. Comparative PL emission spectra of (a) S_P and S_C, (b) S_P and S_T sample.

$$\tau_{avg} = \frac{I_1\tau_1^2 + I_2\tau_2^2}{I_1\tau_1 + I_2\tau_2} \quad (5)$$

On the basis of Equation (5), the average lifetime (τ_{avg}) of samples S_P, S_T, S_C and S_{CT} are determined to be 0.70, 1.47, 1.27 and 2.14 μs (micro-seconds) respectively. Decrease in structural defects due to presence of surfactant during synthesis and lower doping concentration of Tb^{3+} sites in the matrix may affect the $^5D_4 - {}^7F_2$ level emission (when excited under 272 nm wavelength), leading τ_{avg} to be little higher than expected. It is clear from the results that addition of surfactant and their mixture has increased the lifetime of Tb^{3+} doped Y_2O_3 significantly. Presence of surfactant at the time of synthesis decreased the surface defects which decreases the non-radiative decay paths for excited Tb^{3+}. This decreases the non-radiative transition probability which decreases the radiative luminescence emission rate [37]. The decrease in the total transition probability enhances the lifetime of samples prepared by surfactant addition as the lifetime is inverse of the total transition probability [37].

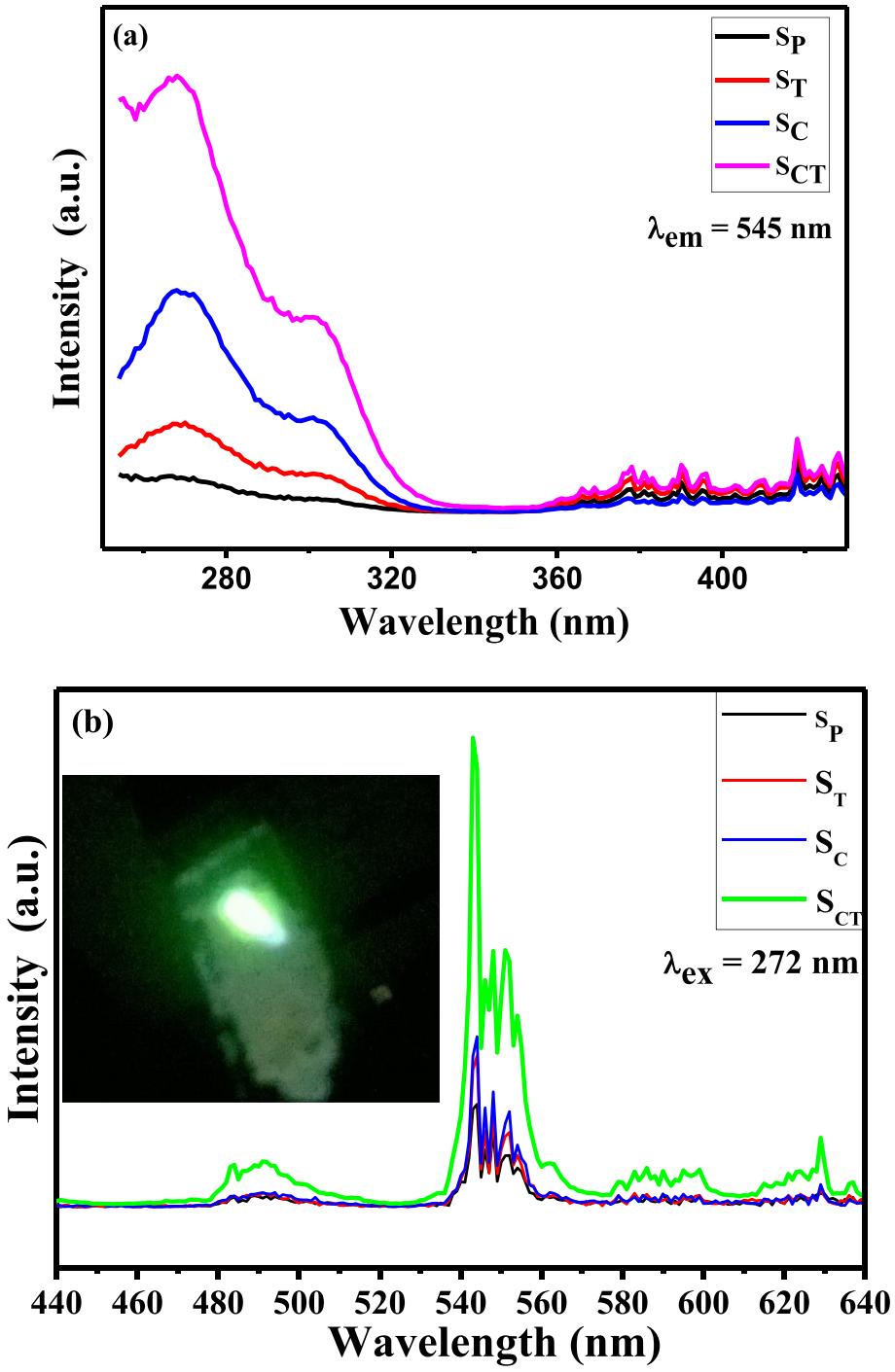

Fig. 8. PL (a) excitation and (b) emission spectra of (a) S_P, (b) S_C, (c) S_T and (d) S_{CT} sample.

3.4.2. Colorimetric studies

The color of any object (self-luminous or reflecting) can be conveniently specified via Commission International de L′ Eclairage (CIE) chromaticity coordinates marked on a chromaticity diagram [38]. Fig. 11 shows the CIE chromaticity coordinates for the optimized sample (S_{CT}) calculated from the emission spectra measured under 272 nm excitation wavelength. The CIE chromaticity coordinates (Fig. 11) for phosphor S_{CT} were found to be (0.340, 0.590) which are very near to ideal green color (0.29, 0.60) [39]. Moreover, the calculated color purity of the sample S_{CT} was found to be 75%. Detailed discussions related to color purity and correlated color temperature calculations are given in supporting data (Section B and Fig. S2).

4. Discussion

In this paper, we made an effort to correlate the XRD and PL studies, so as to understand the effect of surfactants (TOPO and CTAB) on Y_2O_3:Tb^{3+} phosphor. It has been reported earlier that high crystallinity can be obtained in Y_2O_3 phosphors by annealing at higher temperatures in the range of 600–1400 °C [19]. However, with increase in temperature the luminescence along with

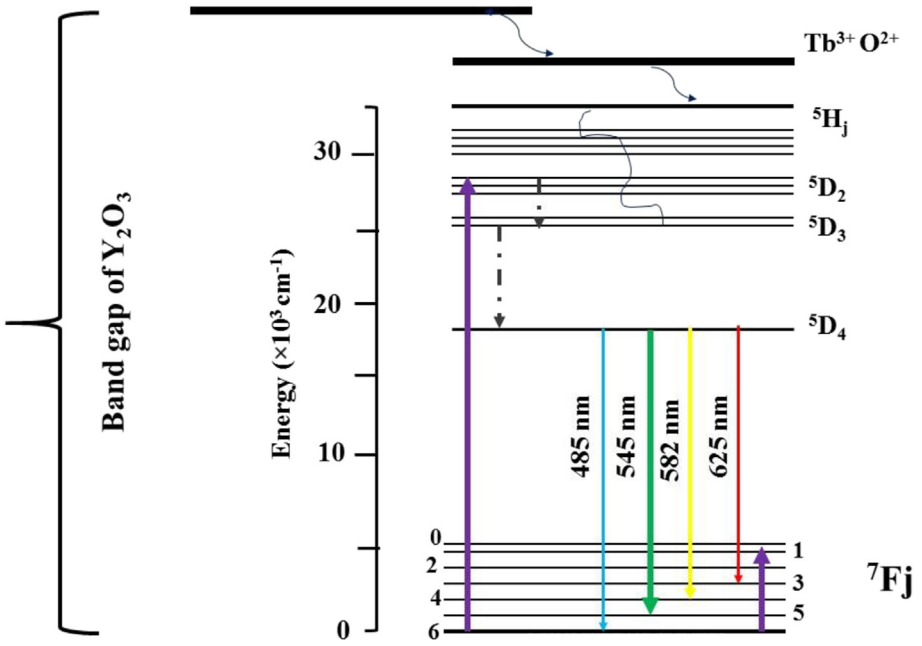

Fig. 9. Band Gap diagram of Tb^{3+} doped Y_2O_3.

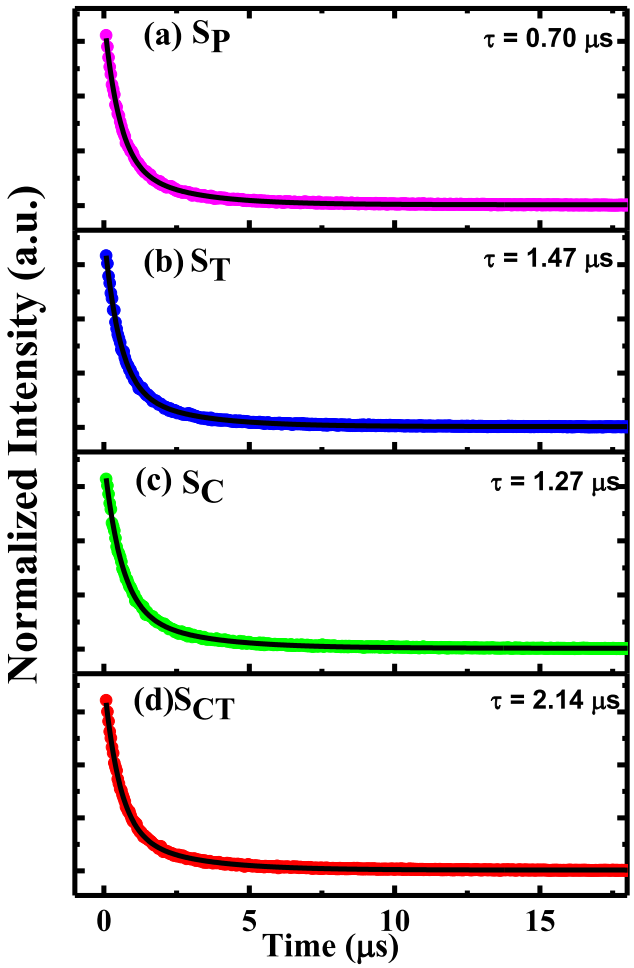

Fig. 10. Luminescence decay curve (λ_{em} = 545 nm) of (a) S_P, (b) S_C, (c) S_T and (d) S_{CT} sample.

crystallinity increases but crystallite size also increases [40]. The main idea to gain better crystalline behavior and small crystalline size of a phosphor is because both these properties upsurge the optical properties of Y_2O_3:Tb^{3+} phosphor [41]. Micro-crystals of highly luminescent and crystalline phosphors are useful in different optoelectronic applications yet restrict their use in different biological applications. Hence, it is required to attain nano-sized particles having high crystallinity and luminescence. Detailed XRD studies have shown that samples of Tb^{3+} doped Y_2O_3 prepared by adding CTAB and TOPO (both) as additives helps in getting better phase stability, crystallinity and smaller crystallite size. XRD studies favors enhancement in PL intensity as samples prepared by adding CTAB surfactant (S_C) has better crystalline behavior as compared to pure sample S_P. Samples prepared by adding TOPO additive (S_T) have shown smaller crystallite size. Both these properties i.e. better crystalline behavior and smaller crystallite size can be observed in sample prepared by adding both TOPO and CTAB samples simultaneously. TEM studies have shown that better morphology in S_C, S_T and S_{CT} play the major role in defending the reason of enhancement in PL emission intensity of these samples as compared to S_P sample. FTIR studies shows that the sample using CTAB + TOPO (i.e. S_{CT}) has fewer amount of nitrate (NO^-) and hydroxyl (OH^-) ions present on its surface in comparison to control sample (S_T) which can be one of the reasons for its increase in the PL intensity. It is well reported that both these NO^{2-} and OH^- ions play as luminescent quenchers which can increase the non-radiative transitions [26,29,42,43]. Overall, the structural and optical properties suggest the optimum use of polymers and their combination during synthesis has resulted in an increase of crystallinity, small particle size and good luminescence together. Although as mentioned above by FTIR studies that the increase of luminescence for S_{CT} sample can be explained by the decrease of luminescence quenchers by using polymers during synthesis. But further work for understanding the detailed mechanism for the role of polymers on structural properties will help the community to use these nanophosphors in diverse applications.

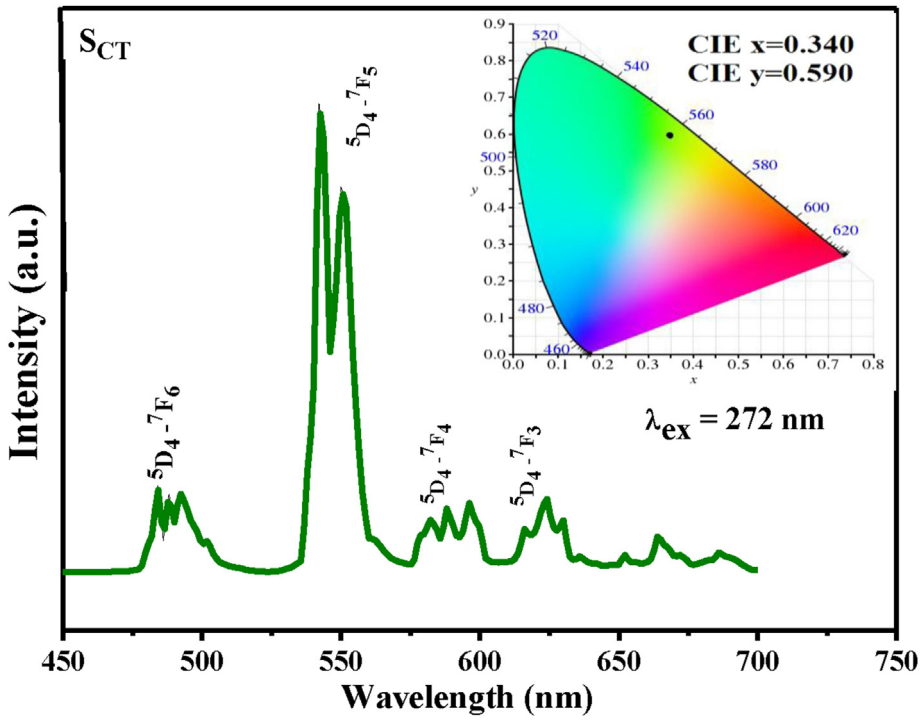

Fig. 11. CIE (x, y) chromaticity diagram of S_{CT} sample.

5. Conclusions

Highly luminescent and green-emitting $Y_2O_3:Tb^{3+}$ nanophosphors were successfully synthesized via a facile technique. Surfactants Cetyl trimethylammonium bromide (CTAB), Trioctylphosphine oxide (TOPO) and their combinations during synthesis has been optimized to get maximum luminescence output. Further, mixed addition of surfactant (CTAB + TOPO) at the time of synthesis has improved crystallinity, morphology, PL emission intensity (~23%) and lifetime of $Y_2O_3:Tb^{3+}$ sample. XRD studies and Rietveld refinement confirmed the body-centered cubic structure of doped phosphors. FTIR studies has also shown significant decrease in hydroxyl and nitrate ions in samples prepared in the presence of surfactants. The Tb^{3+} doped Y_2O_3 phosphor exhibits an intense excitation band ranging from 250 to 400 nm in the near ultraviolet region and produces a bright green emission with the CIE chromaticity coordinates of (0.340, 0.590) which can be used in different applications as a promising green phosphor.

Appendix A. Supplementary data

Supplementary data related to this article can be found at http://dx.doi.org/10.1016/j.jallcom.2016.06.124.

References

[1] C. Feldmann, T. Jüstel, C.R. Ronda, P.J. Schmidt, Inorganic luminescent materials: 100 years of research and application, Adv. Funct. Mater. 13 (2003) 511–516.
[2] D.K. Williams, B. Bihari, B.M. Tissue, J.M. McHale, Preparation and fluorescence spectroscopy of bulk monoclinic Eu3+: Y2O3 and comparison to Eu3+: Y2O3 nanocrystals, J. Phys. Chem. B 102 (1998) 916–920.
[3] E. Goldburt, B. Kulkarni, R. Bhargava, J. Taylor, M. Libera, Size dependent efficiency in Tb doped Y 2 O 3 nanocrystalline phosphor, J. Luminescence 72 (1997) 190–192.
[4] Y. Soo, Z. Ming, S. Huang, Y. Kao, R. Bhargava, D. Gallagher, Local structures around Mn luminescent centers in Mn-doped nanocrystals of ZnS, Phys. Rev. B 50 (1994) 7602.
[5] R. Bhargava, D. Gallagher, T. Welker, Doped nanocrystals of semiconductors-a new class of luminescent materials, J. Luminescence 60 (1994) 275–280.
[6] J. Shen, L.-D. Sun, C.-H. Yan, Luminescent rare earth nanomaterials for bioprobe applications, Dalton Trans. (2008) 5687–5697.
[7] L. Liu, Y. Wang, Y. Bai, X. Zhang, K. Yang, Y. Song, Effects of alkali metal ions on upconversion photoluminescence intensity of Er3+-doped Y2O3 nanocrystals, Appl. Phys. B 110 (2013) 111–115.
[8] Q. Dai, M.E. Foley, C.J. Breshike, A. Lita, G.F. Strouse, Ligand-passivated Eu: Y2O3 nanocrystals as a phosphor for white light emitting diodes, J. Am. Chem. Soc. 133 (2011) 15475–15486.
[9] S. Deng, Z. Xue, Y. Liu, B. Lei, Y. Xiao, M. Zheng, Synthesis and characterization of Y 2 O 2 S: Eu 3+, Mg 2+, Ti 4+ hollow nanospheres via a template-free route, J. Alloys Compd. 542 (2012) 207–212.
[10] y. Chen, x. Yan, q. Liu, x. Wang, morphology and upconversion luminescence of naybf 4: tm 3+ nanocrystals modified by gd 3+ ions, J. Alloys Compd. 562 (2013) 99–105.
[11] R. Bhargava, Doped nanocrystalline materials—physics and applications, J. Luminescence 70 (1996) 85–94.
[12] Y. Soo, S. Huang, Z. Ming, Y. Kao, G. Smith, E. Goldburt, R. Hodel, B. Kulkarni, J. Veliadis, R. Bhargava, X-ray excited luminescence and local structures in Tb-doped Y2O3 nanocrystals, J. Appl. Phys. 83 (1998) 5404–5409.
[13] L.E. Brus, Electron–electron and electron-hole interactions in small semiconductor crystallites: the size dependence of the lowest excited electronic state, J. Chem. Phys. 80 (1984) 4403–4409.
[14] A. Bol, A. Meijerink, Doped semiconductor nanoparticles–a new class of luminescent materials? J. Luminescence 87 (2000) 315–318.
[15] X. Zhang, J. Wang, K. Guo, H. Chen, X. Yang, J. Zhao, Synthesis and luminescence properties of Y 2 O 3: Eu with flower-like microstructure, J. Alloys Compd. 517 (2012) 149–156.
[16] S. Som, S. Sharma, Eu3+/Tb3+-codoped Y2O3 nanophosphors: Rietveld refinement, bandgap and photoluminescence optimization, J. Phys. D Appl. Phys. 45 (2012) 415102.
[17] A.D. French, M.S. Cintrón, Cellulose polymorphy, crystallite size, and the Segal crystallinity index, Cellulose 20 (2013) 583–588.
[18] Q. Wang, J. Guo, W. Jia, B. Liu, J. Zhang, Phase transformation, morphology evolution and luminescence property variation in Y 2 O 3: Eu hollow microspheres, J. Alloys Compd. 542 (2012) 1–10.
[19] Z. Lin-Li, G. Chang-Xin, Z. Jun-Jing, H. Jun-Tao, Photoluminescence of Eu (III)-doped ZnO nanopowder and energy transfer from ZnO to Eu (III) ions, Chin. Phys. Lett. 22 (2005) 1225.
[20] E. Seifert, OriginPro 9.1: scientific data analysis and graphing software—software review, J. Chem. Inf. Model. 54 (2014), 1552–1552.
[21] H. Rietveld, A profile refinement method for nuclear and magnetic structures, J. Appl. Crystallogr. 2 (1969) 65–71.
[22] J. Rodriguez-Carvajal, Full Comput. Program, 2010 (in).
[23] M. Ferrari, L. Lutterotti, Method for the simultaneous determination of anisotropic residual stresses and texture by X-ray diffraction, J. Appl. Phys. 76

(1994) 7246–7255.
[24] T. Ye, Z. Guiwen, Z. Weiping, X. Shangda, Combustion synthesis and photoluminescence of nanocrystalline Y 2 O 3: Eu phosphors, Mater. Res. Bull. 32 (1997) 501–506.
[25] D. Kumar, M. Sharma, O.P. Pandey, Effect of co-doping metal ions (Li+, Na+ and K+) on the structural and photoluminescent properties of nano-sized Y 2 O 3: Eu 3+ synthesized by co-precipitation method, Opt. Mater. 36 (2014) 1131–1138.
[26] Q. Sun, H. Zhao, X. Chen, F. Wang, W. Cai, Z. Jiang, Upconversion emission enhancement in silica-coated Gd 2 O 3: Tm 3+, Yb 3+ nanocrystals by incorporation of Li+ ion, Mater. Chem. Phys. 123 (2010) 806–810.
[27] T. Fan, Q. Zhang, Z. Jiang, The effects of Li on the near-infrared luminescence properties of Nd 3+/Li+ codoped Y 2 O 3 nanocrystals, Opt. Commun. 284 (2011) 1594–1597.
[28] A. Singh, S. Singh, S. Rai, Role of Li+ ion in the luminescence enhancement of lanthanide ions: favorable modifications in host matrices, RSC Adv. 4 (2014) 27039–27061.
[29] K. Mishra, S. Singh, A. Singh, S. Rai, Frequency upconversion in Er 3+ doped Y 2 O 3 nanophosphor: Yb 3+ sensitization and tailoring effect of Li+ ion, Mater. Res. Bull. 48 (2013) 4307–4313.
[30] D. Kumar, M. Sharma, O. Pandey, Morphology controlled Y 2 O 3: Eu 3+ nanophosphors with enhanced photoluminescence properties, J. Luminescence 158 (2015) 268–274.
[31] Y. Lin, Z.-K. Chen, T.-L. Ye, Y.-F. Dai, D.-G. Ma, Z. Ma, Q.-D. Liu, Y. Chen, Novel fluorene-based light-emitting copolymers containing cyanophenyl pendants and carbazole-triphenylamines: synthesis, characterization and their PLED application, Polymer 51 (2010) 1270–1278.
[32] Y. Soo, S. Huang, Y. Kao, V. Chhabra, B. Kulkarni, J. Veliadis, R. Bhargava, Controlled agglomeration of Tb-doped Y2O3 nanocrystals studied by x-ray absorption fine structure, x-ray excited luminescence, and photoluminescence, Appl. Phys. Lett. 75 (1999) 2464–2466.
[33] X.-Y. Sun, M. Gu, S.-M. Huang, X.-L. Liu, B. Liu, C. Ni, Enhancement of Tb 3+ emission by non-radiative energy transfer from Dy 3+ in silicate glass, Phys. B Condens. Matter 404 (2009) 111–114.
[34] X. Liu, L. Yan, J. Lin, Synthesis and luminescent properties of LaAlO3: RE3+ (RE= Tm, Tb) nanocrystalline phosphors via a sol—gel process, J. Phys. Chem. C 113 (2009) 8478–8483.
[35] M. Yu, J. Lin, J. Fang, Silica spheres coated with YVO4: Eu3+ layers via sol-gel process: a simple method to obtain spherical core-shell phosphors, Chem. Mater. 17 (2005) 1783–1791.
[36] M. Ilmer, B. Grabmaier, G. Blasse, Luminescence of Bi3+ in gallate garnets, Chem. Mater. 6 (1994) 204–206.
[37] R.M. Bakker, H.-K. Yuan, Z. Liu, V.P. Drachev, A.V. Kildishev, V.M. Shalaev, R.H. Pedersen, S. Gresillon, A. Boltasseva, Enhanced localized fluorescence in plasmonic nanoantennae, Appl. Phys. Lett. 92 (2008) 043101.
[38] J.S. Kumar, K. Pavani, A.M. Babu, N.K. Giri, S. Rai, L.R. Moorthy, Fluorescence characteristics of Dy 3+ ions in calcium fluoroborate glasses, J. Luminescence 130 (2010) 1916–1923.
[39] D.H. Brainard, Calibration of a computer controlled color monitor, Color Res. Appl. 14 (1989) 23–34.
[40] W.-N. Wang, W. Widiyastuti, T. Ogi, I.W. Lenggoro, K. Okuyama, Correlations between crystallite/particle size and photoluminescence properties of submicrometer phosphors, Chem. Mater. 19 (2007) 1723–1730.
[41] A. Boukerika, L. Guerbous, Annealing effects on structural and luminescence properties of red Eu 3+-doped Y 2 O 3 nanophosphors prepared by sol–gel method, J. Luminescence 145 (2014) 148–153.
[42] T. Fan, Q. Zhang, Z. Jiang, Enhanced near-infrared luminescence in Y 2 O 3: Yb nanocrystals by codoping with Li+ ion, Opt. Commun. 284 (2011) 249–251.
[43] D. Li, Y. Wang, X. Zhang, H. Dong, L. Liu, G. Shi, Y. Song, Effect of Li+ ions on enhancement of near-infrared upconversion emission in Y2O3: Tm3+/Yb3+ nanocrystals, J. Appl. Phys. 112 (2012) 094701.